

Optical Readout of Reconfigurable Layered Magnetic Domain Structure in CrSBr

Aleksandra Łopion^{1*}, Pierre-Maurice Piel¹, Manuel Terbeck¹,
Jan-Hendrik Larusch¹, Jakob Henz¹, Marie-Christin Heißenbüttel²,
Kseniia Mosina³, Thorsten Deilmann², Michael Rohlfing²,
Zdenek Sofer³, Ursula Wurstbauer^{1*}

¹Physikalisches Institut and Center for Soft Nanoscience (SoN), University of Münster, Wilhelm Klemm Str. 10, Münster, 48149, Germany.

²Institut für Festkörpertheorie, University of Münster, Wilhelm Klemm Str. 10, Münster, 48149, Germany.

³University of Chemistry and Technology, Technicka 5, Prague, 16628, Czech Republic.

*Corresponding author(s). E-mail(s): alopion@uni-muenster.de;
wurstbauer@uni-muenster.de;

Abstract

The emergence of intelligent matter has sparked significant interest in next-generation technologies. We report on the discovery of a reconfigurable magnetic multilayer domain structure in the van der Waals magnet CrSBr, exhibiting a unique combination of magnetic and optical properties. Applying an external magnetic field along the easy axis drives the hysteretic antiferromagnetic-to-ferromagnetic transition that is not universally binary, but instead develops through a cascade of intermediate magnetic configurations whose multiplicity and stability scale systematically with thickness. This material can be considered as a prototypical intelligent matter, capable of encoding, processing, and storing information through its tunable magnetic structure. The directly linked optical properties of CrSBr, modulated by the magnetic structure, provide a readout mechanism for the stored information compatible with modern information distribution using light. With its adaptive properties, CrSBr is an attractive candidate for neuromorphic circuitries, enabling the design of brain-inspired computing architectures that can learn and evolve in response to changing environments.

Keywords: van der Waals magnets, CrSBr, reconfigurable magnetic system, adaptive layered magnetic domains, optical readout, metastable magnetic states

1 Introduction

The discovery of long-range magnetic order in atomically thin crystals demonstrated that the Mermin–Wagner theorem does not hold for two-dimensional (2D) magnetic structures embedded in a three dimensional environment [1–3]. 2D layered magnetic structures offer rich and tunable long-range order due to highly anisotropic intra- and interlayer exchange interactions together with weak van der Waals (vdW) interaction allowing for interfacial engineering and control by external stimuli [2–7].

Reconfigurability, together with hysteresis, meaning that the magnetization in a magnet depends on its history, is attractive for information technologies enabling writing and storage of information. In this regard, antiferromagnets (AFM) offer ultrafast dynamics and multistability, while ferromagnets (FM) provide binary states but may suffer from magnetostatic (dipolar) crosstalk [8–10]. Encoding information in optically accessible AFM-derived states therefore opens pathways towards memory functionalities, spin-driven optoelectronics or even neuromorphic architectures. The latter requires that a system is capable to learn, process, store and distribute information by interacting with its environment, a combination of functionalities often referred to as “intelligent matter” [11]. While writing and storage of digital information is at the heart of a magnetic systems with long-range order, learning capabilities, distribution of information and universal readout are often challenging.

In two-dimensional vdW magnets, the AFM and FM functionalities become especially useful because anisotropy, carrier density, and interlayer exchange can be tuned by gating, strain, or stacking, enabling deterministic stabilization and on-demand switching between AFM and FM phases and more exotic long-range order patterns [12–15]. In this regard, CrSBr, as an environmentally stable magnetic semiconductor, stands out among two-dimensional magnets as a system featuring ferromagnetic interaction within each layer and antiferromagnetic correlation between adjacent layers [16]. Consequently, magnetic order directly reshapes the underlying electronic states and their excitations such as excitons [16–19]. Excitons are Coulomb-coupled electron–hole pairs that can couple to light by their dynamic dipole connecting spin order and reshaped electronic states to light — a degree of freedom used in modern technologies to read out and distribute information [6, 20–23].

With a direct bandgap of around 1.3 eV and an unusually high refractive index near its excitonic resonances, even tens-of-nanometers thick flakes exhibit pronounced interference effects dictated by van der Waals stacking rather than external nanofabrication [24–26]. Here, we establish CrSBr as a naturally reconfigurable magneto-optical resonator enabling optical readout of a layer-by-layer magnetic domain structure that is controlled by external stimuli. The combined experimental and simulation results highlight the “intelligent matter” capability of the vdW magnetic semiconductor CrSBr.

2 Results

In Figure 1, the linear optical response of CrSBr at a temperature of 4 K is shown tracing the magnetic-field-driven switching from AFM over an intermediate magnetic state (iMS) to the FM state. Application of an external magnetic field B along the

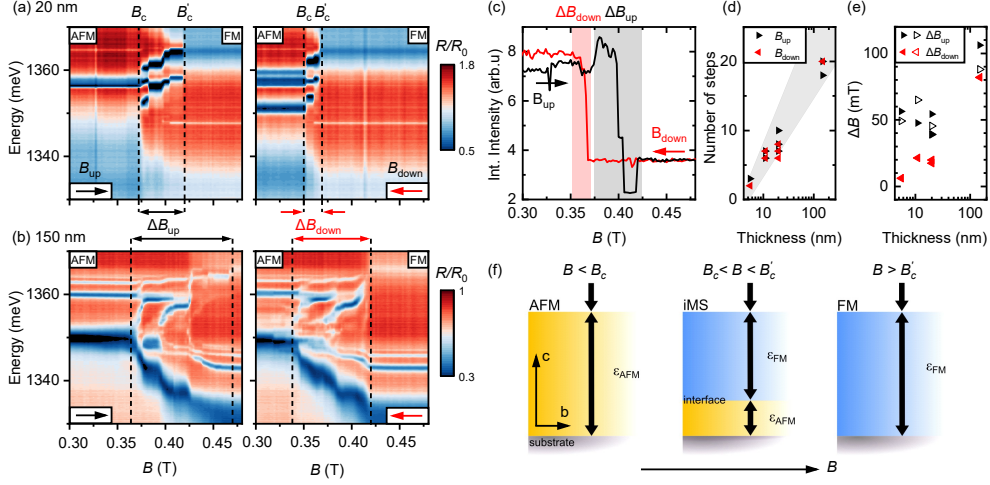


Fig. 1 Thickness dependence of field-driven optical switching in CrSBr. Magneto-reflectance spectra R/R_0 with B applied along the easy (b) axis. The reflectance ratio R/R_0 is color-coded. Shown are magnetic field B_{up} and B_{down} sweeps for (a) 20 nm thick CrSBr and (b) for 150 nm thick CrSBr. Vertical dashed lines separate AFM, iMS, and FM phases and indicate the critical switching fields B_c between AFM and iMS and B'_c , between iMS and FM. (c) Integrated R/R_0 reflectance ratio (between 1364.1 and 1365.3 meV — range for the exciton in AFM state) for 20 nm CrSBr for up B_{up} and down B_{down} sweep with iMS windows marked by the shaded regions. (d) Number of steps in the iMS region as a function of layer thickness for up- and down-sweep in semi-logarithmic representation. (e) Magnetic field range ΔB of the iMS phase for up- and down-sweep as a function of layer thickness in semi-logarithmic representation. Full symbols stem from reflectance and open from PL spectra. (f) Schematic dielectric profiles for alternating ε_{AFM} (AFM), mixed AFM/FM stack (iMS), and uniform ε_{FM} (FM).

crystal's easy axis b drives step-like switching between AFM and FM order with distinct intermediate configurations directly visible in the optical spectra. A few discrete jumps appear in the magneto-reflectance spectra for a 20 nm thick CrSBr flake consisting of 25 layers, assuming a monolayer thickness of $d_{\text{ML}} \approx 0.78 \text{ nm}$ [27, 28], whereas a whole cascade of changes emerges for a bulk-like 150 nm thick flake. Both, the energy and the reflectance ratio for the given energy are highly sensitive to the different iMS states. The integrated reflectance ratio in the energy range of the exciton in the AFM state for the 20 nm CrSBr is shown in Figure 1(c) for magnetic-field up- (black) and down-sweeps (red). The iMS window is marked for both traces by the shaded area. While the overall iMS signatures in the spectra emerge in both magnetic-field up- and down-sweeps as displayed in Figure 1(a,b), integrated reflectance ratio R/R_0 , number of steps and magnetic field window ΔB are dependent on the sweep direction and hence on the path of the magnetic phase transition [Figure 1(c–e)]. Additionally, the critical fields B_c and B'_c exhibit the well-known hysteresis for switching along the magnetic easy axis [6, 29–31]. The critical fields B_c and B'_c separate the iMS region from AFM and FM configurations, respectively, and quantify the iMS window by $\Delta B = B'_c - B_c$. The iMS region reveals numerous intermediate states and shows hysteretic behaviour between up- and down-sweep with a drastic difference in

the magnetic field window with $\Delta B_{\text{up}} > \Delta B_{\text{down}}$. It is clearly visible that the iMS window is significantly different for up- and down-sweep, both in terms of critical fields B_c , B'_c and the width of the B-field window ΔB . The width is reduced for down-sweep compared to up-sweep and the critical fields are additionally lowered as expected from hysteretic behaviour of magnetization along an easy axis. By comparing various samples of different thicknesses we observe that those trends are universal (see Supplementary Fig. 3), however, the number of steps in the iMS range, as well as the ΔB and values for critical fields increase with increasing layer thickness. The data are summarized in Figures 1(d,e) and hold for magneto-reflectance and magneto-photoluminescence (PL) measurements. The combined findings suggest metastable magnetic configurations providing a memory function that is not only responsive but even adaptive with respect to external B -field stimuli. In the optical reflectance spectra the appearance of such intermediate magnetic configurations manifests as a drastic change of the optical response, with the emergence of new spectral features in the spectra and subsequent blueshift of reflectance bands upon increase of the external magnetic field.

The evolution of the spectra in the iMS configuration confirms multi-step layer-by-layer switching from AFM to FM and vice versa driven by the external field [16, 32, 33]. This layer-by-layer switching turns the homogeneous AFM or FM vdW stack into a multilayered out-of-plane magnetic domain system with alternating AFM and FM domains of variable thickness. This allows multiple intermediate metastable magnetic configurations due to the competing contributions of interlayer exchange interactions, anisotropy, and Zeeman effect. The multilayer domain structure is schematically shown on example of one possible configuration in Figure 1(f). We would like to point out that many more configurations with multiple interfaces between AFM and FM domains exist. The distinct optical response enables a rigorous optical readout of layer-by-layer spin reconfiguration that differs for up- and down-sweep allowing to trace the controlled manipulation of the layered magnetic domains and the creation of metastable reconfigurable states.

The microscopic origin of the sensitivity of the optical spectra to the long-range magnetic order and hence the out-of-plane domain structure in the iMS is the magnetization-dependent spatial extent of the relevant electronic states. In antiferromagnetic alignment the electronic wave-functions and so the exciton is confined in a single monolayer due to suppressed interlayer hopping. The dielectric response of the exciton is thus monolayer-like and the exciton energy is higher due to the higher single-particle energy [34]. In the ferromagnetic configuration, parallel alignment permits interlayer tunneling, delocalizing the electronic and hence excitonic states across ~ 5 layers and lowering their energies [34]. For the ferromagnetic stacks thinner than these 5 layers, the exciton energy is expected to occur between the monolayer-like AFM and bulk-FM limits due to quantum confinement. This combined impact of the magnetization on the spectral response primarily gives rise to the sensitivity of the exciton energy to the magnetic ordering and directly links the change of the complex dielectric function with $\varepsilon_{\text{AFM}}(\omega) \neq \varepsilon_{\text{FM}}(\omega)$. In the case of multilayered CrSBr flakes, such as the 20 and 150 nm samples, consisting respectively 25 and 193 individual layers (discussed in Figure 1), the iMS regime is very rich. A successive subset

of layers can flip nearly independently from AFM to FM or vice versa resulting in the introduced layered magnetic domain structure characteristic for the iMS turning the system simultaneously into an optical multilayer system analogue to optical superlattices [35–39].

The schematic in Figure 1(f) illustrates how the layered magnetic domain structure in the iMS regime is linked to an optical multilayer system rendering it into a magnetic-field-reconfigurable optical metamaterial. When an external magnetic field along the CrSBr's easy axis reaches values near the critical values B_c or B'_c , the magnetic order in the multilayer stack flips to a different configuration, which in most cases is neither a pure AFM nor FM state, rather a mixed AFM–FM stack as already introduced and labeled iMS. Because $\epsilon_{\text{AFM}} \neq \epsilon_{\text{FM}}$, this reconfiguration of the magnetic order in the stack leaves discrete optical fingerprints that unambiguously identify AFM, FM, and the different iMS configurations. Each change of the magnetic order initiated by the external magnetic field modifies the thickness and alternation of the dielectric layers in the stack and thus its optical response by light-guiding effects.

Previous studies have identified several excitonic resonances in CrSBr, including energetically close-lying bulk excitons and a surface-confined state [23]. The microscopic origin of the experimentally observed resonances remains a topic of active research. They all exhibit rather sharp resonances and a strong oscillator strength that couples efficiently to light. As a result, even few-layer flakes show optical spectra that are shaped, not only by the intrinsic exciton responses, but also by light-guiding effects within the layered crystal eventually even causing hybridization in thicker stacks with the response commonly described in a polariton framework [24]. In practice, this means that excitonic resonances in multilayer CrSBr are never observed in isolation, but always in a form modified by the surrounding dielectric environment of the flake not only modifying exciton binding energies [40], but even more importantly give rise to interference effects by the light propagating in these multilayer systems.

We validate the suggested light-guiding mechanism in conjunction with the magnetic field–written magnetic layered domain structure as the origin of the abrupt changes in energy and intensity in the optical spectra through transfer-matrix-method (TMM) simulations. In Figure 2, simulated and measured reflectance spectra are compared side-by-side for a 25L-CrSBr stack. Spectra for different magnetic field–written iMS domain structures starting with the AFM case followed by the iMS situation with increasing FM contribution in the layer sequence until the FM situation is reached are contrasted. The simulated data reproduce the key signatures in the experimental spectra such as the numbers of steps, energy and intensity modulations extremely well.

The TMM simulations are based on a minimal model using a single Lorentzian oscillator in $\epsilon(\omega)$, representing the main excitonic resonance, whose frequency redshifts abruptly when the system transitions from AFM to FM order, in agreement with experiment and theory [16, 34]. We neglected the contribution of high-lying excitons to the dielectric function $\epsilon(\omega)$ as they are far off the investigated spectral range and a preliminary test showed that their contribution is negligible in the TMM. In turn, we limit the TMM to only one well-established excitonic resonance in $\epsilon(\omega)$ in the

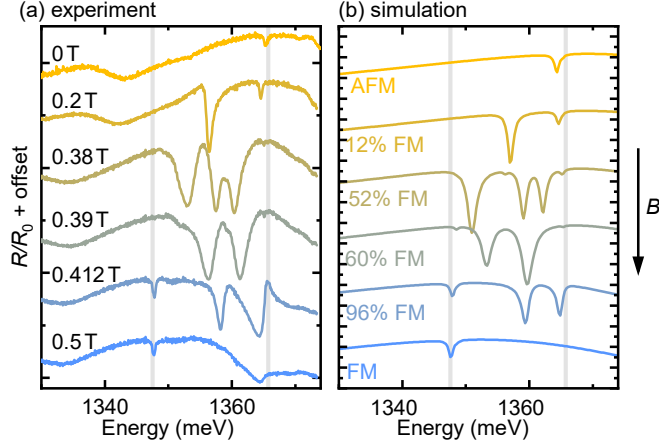


Fig. 2 Comparison of experimental and simulated spectra for 25-layer CrSBr. (a) Experimental magneto-reflectance spectra R/R_0 for selected magnetic field values for the field applied along the CrSBr easy axis, where 0 T and 0.5 T correspond to AFM and FM order and all values in between to an iMS state; traces are offset for clarity. (b) Simulated magneto-reflectance spectra using the TMM based on layered magnetic domains for AFM, FM and representative iMS, with increasing number of FM layers (given in %). Simulations are purely based on $\varepsilon_{\text{AFM}}(\omega)$, $\varepsilon_{\text{FM}}(\omega)$ and layer thickness and not fitted to experimental data.

investigated spectral range. We find that between the pure AFM and FM situation in the stack, the simulated spectra evolve from a single mode into a ladder of modes.

Grey vertical lines shown in the experimental and simulated spectra in Figures 2(a,b) mark the exciton energies in the AFM and FM phases, making it explicit that the observed mode shifts follow the exciton's magnetic response.

Having established the occurrence of the iMS regime with its peculiar fingerprints in optical spectra together with hysteretic switching behaviour marked by the sweep-dependency of the signatures, critical fields B_c , B'_c and their magnetic field window ΔB ranging from a few tens of monolayers towards bulk, we now turn to the ultra-thin sample regime. We discuss this regime using the example of a 7-layer CrSBr film with a layer thickness of approximately 5.5 nm, as determined by atomic force microscopy. As contrasted in Figures 3(a) and (b), the magnetic-field-dependent evolution of the magneto-reflectance spectra differs again significantly between up- and down-sweeps for these very thin layers. While the up-sweep exhibits the established transition from AFM to iMS and finally to FM order, characterized by two critical fields, B_c and B'_c , separating these regions, which are marked by distinct spectral signatures, the spectral evolution for the down-sweep reveals only one critical field, $B_c = B'_c$, consistent with a direct phase transition from FM to AFM. In other words, the experimental findings for the up-sweep are consistent with the switching of an iMS with layer-by-layer switching accompanied by the formation of layered magnetic domains, whereas magnetic domain formation is absent for the down-sweep. Representative experimental reflectance spectra for FM, iMS and AFM states are shown in Figure 3(c). In the iMS range of the up-sweep, we observe the coexistence of spectral signatures belonging to excitons in both antiferromagnetic (AFM) and ferromagnetic

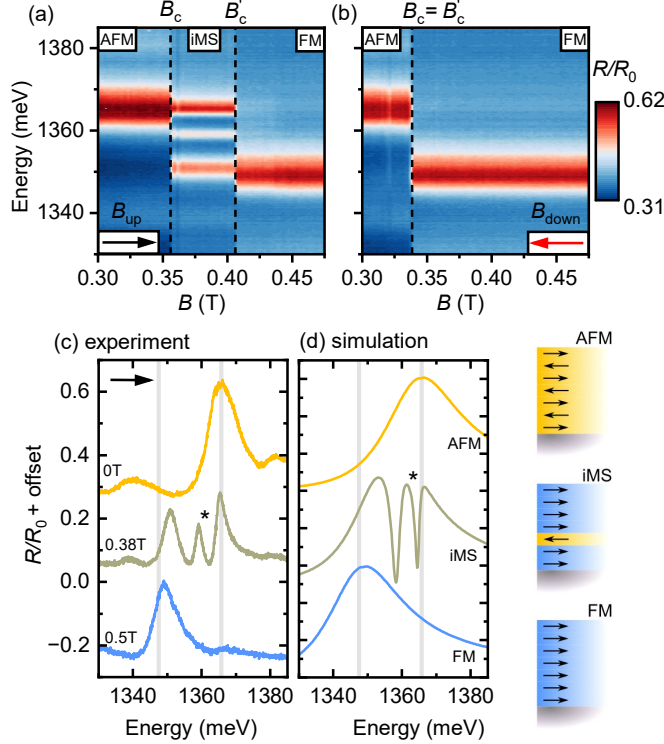


Fig. 3 Magneto-reflectance investigation for 7-layer CrSBr as the lower limit for layered-magnetic domain formation. Magneto-reflectance R/R_0 spectra for a 7L-CrSBr flake; (a) up-sweep, B_{up} , (b) down-sweep, B_{down} . Vertical dashed lines indicate critical switching fields. (c) Selected reflectance spectra for AFM, iMS and FM state for B_{up} . The asterisk (*) marks an additional resonance that appears only within the intermediate-state window for B_{up} . (d) Simulated magneto-reflectance spectra using the TMM for pure AFM, pure FM and iMS (4L FM, 1L AFM, 2L FM) configuration depicted at the right.

(FM) configurations, as well as an additional resonance located energetically between them. The additional mode, marked by an asterisk (*) in Figure 3(c) can only be reproduced in TMM simulations (Figure 3(d)) by including an additional resonance, in contrast to TMM simulations for thicker films, where the experimental signatures are accurately replicated by considering only AFM and FM layers. The required intermediate resonance needs to be energetically between the AFM and FM excitons. This is in agreement with the fact that for an FM layer with a thickness of fewer than 5 layers, the exciton energy increases due to quantum confinement, approaching the limit of the AFM case in the monolayer limit. While the existence of FM domains with fewer than 5 layers is expected to be unfavorable in thicker films consistent with the excellent agreement between experimental data and TMM simulations, the thickness effect cannot be neglected in the few-layer limit. In line with this consideration, for 7L CrSBr a metastable iMS domain configuration composed of six FM layers and one AFM layer in between, as sketched in Figure 3(e), can explain the experimental findings, as corroborated by the corresponding TMM model simulation. Other

microscopic origins such as additional excitonic species cannot be fully excluded, but contradict the reproducible absence of this additional resonance for the magnetic-field down-sweep and are not covered by existing theory [34]. The reduced exciton localization in the FM order compared to the AFM layer may in general contribute to the asymmetry between up- and down-sweeps ($\Delta B_{\text{up}} \neq \Delta B_{\text{down}}$), which is corroborated by the fact the effect is layer dependent and favours the direct switching from FM to AFM (down-sweep) for the 7L limit.

The rich evolution of the optical response of CrSBr under application of an external magnetic field along the easy axis can be well understood by the introduced magnetic multilayer model. This understanding arises from a multifaceted interplay of magnetic exchange interactions leading to layer-by-layer switching controlling a tunable metastable layered magnetic domain structure in the iMS. The iMS exhibits pronounced hysteresis and is characterized by different critical fields B_c , B'_c and magnetic field window ΔB for the phase transitions from AFM to FM and vice versa. Both transitions display the iMS, although it is less pronounced for the transition from FM to AFM and disappears for 7 layers. However, the iMS still exists for the AFM to FM transition at this lower layer number limit. This magnetic reconfigurability, with its responsive nature, adaptive optical properties, and information storage capability controlled by an external field, makes CrSBr not only an intriguing optical metamaterial but also exhibits all the characteristics necessary to be considered as intelligent matter [11].

The optical properties of these various iMS with rich magnetic domain structures can be well reproduced by light-guiding through a multilayer model. This model considers a sequence of alternating AFM and FM layers of variable thickness, whose optical properties are described by $\varepsilon_{\text{AFM}}(\omega)$ and $\varepsilon_{\text{FM}}(\omega)$. These are determined solely by a single strong and sharp excitonic resonance with different energies in the AFM and FM cases.

With these ingredients, TMM simulations describing light propagation through the layer stack, including interference effects from light reflected from different interfaces, can accurately reproduce the experimentally determined magneto-reflectance spectra for various sample thicknesses within a unified framework. There is no need to invoke additional exciton species or other hybrid particles. The only exception is the limit of ultra-thin films, where quantum confinement of the electronic and hence excitonic states must be taken into account. This approach allows for the optical tracking of layer-by-layer switching and characterization of the layered magnetic domains through relatively simple optical experiments such as reflectance and PL spectroscopies.

The tunability of the optical response by the magnetic layer structure is beneficial for generating a targeted response, as required for optical metamaterials. Even more promisingly, the optical properties can serve as a sensitive readout of the magnetic multilayer domain structure. We expect that this peculiar and metastable state, which is fully reconfigurable, can be written not only by an external magnetic field but also by other stimuli, such as suitable optical, electrical, or microwave pulses, causing switches, for example, via coupling of different degrees of freedom through their collective excitations, such as magnons, phonons, and other excitations such as excitons [6, 7, 12].

3 Methods

3.1 Sample preparation.

CrSBr flakes were mechanically exfoliated from bulk crystals onto Si substrates with a 100-nm SiO₂ layer. Flake thicknesses were verified by atomic force microscopy (AFM).

3.2 Optical measurements.

All experiments were performed at 4 K in a closed-cycle cryostat equipped with optical access and superconducting magnets. The detection axis was aligned along the crystallographic b-axis of CrSBr, which exhibits a strong optical response, while the orthogonal axis yields negligible signal. PL was excited with a continuous-wave 532-nm laser. Reflectance spectra were acquired using a laser-driven broadband white-light source. Both PL and reflectance were collected in a backscattering geometry with linear polarization selection and dispersed in a spectrometer.

3.3 Magnetic field configuration.

Magnetic fields were applied along the easy axis of CrSBr, with values up to 0.5 T. The step size in magnetic field was 0.002 T. For comparison, measurements were also performed with the field along the intermediate a-axis, up to 3 T, confirming the expected anisotropy; these data are delivered as supplementary information.

3.4 Data analysis.

Spectra were background-corrected and normalized to a reference signal from the bare substrate.

3.5 Modeling.

The multilayer optical response was simulated with the transfer-matrix method (TMM). AFM- and FM-aligned layers were assigned distinct dielectric functions, $\epsilon_{\text{AFM}}(\omega)$ and $\epsilon_{\text{FM}}(\omega)$, each containing a single Lorentz oscillator; background indices and oscillator strengths were fixed to the same value. The only free parameters were the resonance energies in the AFM and FM cases, which were obtained by fitting the reflectance signal obtained for the thick flake at low-field (AFM) and high-field (FM), respectively. To capture the few-layer regime, we introduced an explicit thickness dependence of the FM exciton energy, $E_X^{\text{FM}}(N)$, which decreases with the ferromagnetic slab thickness N and saturates for $N \gtrsim 5$ monolayers (bulk-like limit). The exact values for $E_X^{\text{FM}}(N)$ and other parameters used for calculations are given in the supplementary information, along with the comparison to the simplified model without taking $E_X^{\text{FM}}(N)$ into account for thin-layers regime. Both reproduce the multiplication of modes and their abrupt field-induced rearrangements. We did not model the magnetization dynamics. Instead, we assumed that the ferromagnetic phase fraction in the stack increases monotonically with the applied field.

Supplementary Information. See Supplementary Information for additional methods, figures, and tables.

Acknowledgements. The authors gratefully acknowledge financial support by the German Science Foundation (DFG) via Grants No. 443274199 and 556436549 (WU 637/7-2,8-1), and the priority program 2244 (2DMP) through start-up funding. This project has received funding from the European Union’s Horizon Europe research and innovation program under grant agreement No. 101130224 “JOSEPHINE”. T.D. acknowledges financial support from the Deutsche Forschungsgemeinschaft (DFG, German Research Foundation) through Project No. 426726249 (DE 2749/2-1 and DE 2749/2-2). The authors gratefully acknowledge the Gauss Centre for Supercomputing e.V. (www.gauss-centre.eu) for funding this project by providing computing time through the John von Neumann Institute for Computing (NIC) on the GCS Supercomputer JUWELS at Jülich Supercomputing Centre (JSC) [41]. Z.S. was supported by project LUAUS25268 from the Ministry of Education, Youth and Sports (MEYS) and by the project Advanced Functional Nanorobots (reg. No. CZ.02.1.01/0.0/0.0/15_003/0000444 financed by the EFRR) and by the ERC-CZ program (project LL2101) from Ministry of Education, Youth and Sports (MEYS). Z.S. acknowledges the assistance provided by the Advanced Multiscale Materials for Key Enabling Technologies project, supported by the Ministry of Education, Youth, and Sports of the Czech Republic. Project No. CZ.02.01.01/00/22_008/0004558, Co-funded by the European Union.

References

- [1] Mermin, N. D. & Wagner, H. Absence of ferromagnetism or antiferromagnetism in one- or two-dimensional isotropic Heisenberg models. *Physical Review Letters* **17**, 1133–1136 (1966).
- [2] Gong, C. *et al.* Discovery of intrinsic ferromagnetism in two-dimensional van der Waals crystals. *Nature* **546**, 265–269 (2017).
- [3] Huang, B. *et al.* Layer-dependent ferromagnetism in a van der Waals crystal down to the monolayer limit. *Nature* **546**, 270–273 (2017).
- [4] Gong, C. & Zhang, X. Two-dimensional magnetic crystals and emergent heterostructure devices. *Science* **363**, eaav4450 (2019).
- [5] Blei, M. *et al.* Synthesis, engineering, and theory of 2D van der Waals magnets. *Applied Physics Reviews* **8**, 021301 (2021).
- [6] Tabataba-Vakili, F. *et al.* Doping-control of excitons and magnetism in few-layer CrSBr. *Nature Communications* **15**, 4735 (2024).
- [7] Bae, J. *et al.* Exciton–magnon coupling in a 2D magnet. *Nature* **609**, 282–286 (2022).
- [8] Jungwirth, T., Marti, X., Wadley, P. & Wunderlich, J. Antiferromagnetic spintronics. *Nature Nanotechnology* **11**, 231–241 (2016).

- [9] Baltz, V. *et al.* Antiferromagnetic spintronics. *Reviews of Modern Physics* **90**, 015005 (2018).
- [10] Žutić, I., Fabian, J. & Das Sarma, S. Spintronics: Fundamentals and applications. *Reviews of Modern Physics* **76**, 323–410 (2004).
- [11] Kaspar, C., Ravoo, B. J., van der Wiel, W. G., Wegner, S. V. & Pernice, W. H. The rise of intelligent matter. *Nature* **594**, 345–355 (2021).
- [12] Cenker, J. *et al.* Reversible strain-induced magnetic phase transition in a van der Waals magnet. *Nature Nanotechnology* **17**, 256–261 (2022).
- [13] Deng, Y. *et al.* Gate-tunable room-temperature ferromagnetism in two-dimensional Fe_3GeTe_2 . *Nature* **563**, 94–99 (2018).
- [14] Chen, W. *et al.* Direct observation of van der Waals stacking-dependent interlayer magnetism. *Science* **366**, 983–987 (2019).
- [15] Song, T. *et al.* Direct visualization of magnetic domains and moiré magnetism in twisted 2D magnets. *Science* **374**, 1140–1144 (2021).
- [16] Wilson, N. P. *et al.* Interlayer electronic coupling on demand in a 2D magnetic semiconductor. *Nature Materials* **20**, 1657–1662 (2021).
- [17] Klein, J. *et al.* The bulk van der waals layered magnet crsbr is a quasi-1d material. *ACS nano* **17**, 5316–5328 (2023).
- [18] Komar, R. *et al.* Colossal magneto-excitonic effects in 2d van der Waals magnetic semiconductor CrSBr. *arXiv preprint arXiv:2409.00187* (2024).
- [19] Smiertka, M. *et al.* Unraveling the nature of excitons in the 2D magnetic semiconductor CrSBr. *arXiv preprint arXiv:2506.16426* (2025).
- [20] Wang, G. *et al.* Colloquium: Excitons in atomically thin transition metal dichalcogenides. *Reviews of Modern Physics* **90**, 021001 (2018).
- [21] Tagarelli, F. *et al.* Electrical control of hybrid exciton transport in a van der Waals heterostructure. *Nature Photonics* **17**, 615–621 (2023).
- [22] Diederich, G. M. *et al.* Exciton dressing by extreme nonlinear magnons in a layered semiconductor. *Nature Nanotechnology* **20**, 617–622 (2025).
- [23] Shao, Y. *et al.* Magnetically confined surface and bulk excitons in a layered antiferromagnet. *Nature Materials* 1–8 (2025).
- [24] Dirnberger, F. *et al.* Magneto-optics in a van der Waals magnet tuned by self-hybridized polaritons. *Nature* **620**, 533–537 (2023).

- [25] Wang, T. *et al.* Magnetically-dressed CrSBr exciton-polaritons in ultrastrong coupling regime. *Nature Communications* **14**, 5966 (2023).
- [26] Diederich, G. M. *et al.* Tunable interaction between excitons and hybridized magnons in a layered semiconductor. *Nature Nanotechnology* **18**, 23–28 (2023).
- [27] Lee, K. *et al.* Magnetic order and symmetry in the 2D semiconductor CrSBr. *Nano Letters* **21**, 3511–3517 (2021).
- [28] Pellet-Mary, C. *et al.* Lateral exchange bias for Néel-vector control in atomically thin antiferromagnets. *Nature Communications* **16**, 9725 (2025).
- [29] Stoner, E. C. & Wohlfarth, E. P. A mechanism of magnetic hysteresis in heterogeneous alloys. *Philosophical Transactions of the Royal Society A* **240**, 599–642 (1948).
- [30] Dieny, B. *et al.* Perpendicular magnetic anisotropy at transition metal/oxide interfaces and beyond. *Reviews of Modern Physics* **89**, 025008 (2017).
- [31] Boix-Constant, C. *et al.* Programmable magnetic hysteresis in orthogonally-twisted CrSBr building blocks. *Advanced Materials* (2025).
- [32] Krelle, L. *et al.* Magnetic correlation spectroscopy in CrSBr. *ACS nano* **19**, 33156–33163 (2025).
- [33] Alapatt, V. *et al.* Highly polarized single-photon emission from localized excitons in a WSe₂/CrSBr heterostructure. *ACS photonics* **12**, 3024–3031 (2025).
- [34] Heißenbüttel, M.-C. *et al.* Quadratic optical response to a magnetic field in the layered magnet CrSBr. *Physical Review B* **111**, 075107 (2025).
- [35] Yablonovitch, E. Inhibited spontaneous emission in solid-state physics and electronics. *Physical Review Letters* **58**, 2059–2062 (1987).
- [36] Fink, Y. *et al.* A dielectric omnidirectional reflector. *Science* **282**, 1679–1682 (1998).
- [37] Dufferwiel, S. *et al.* Exciton-polaritons in van der Waals heterostructures embedded in tunable microcavities. *Nature Communications* **6**, 8579 (2015).
- [38] Ścieśiek, M. *et al.* Long-distance coupling and energy transfer between exciton states in magnetically controlled microcavities. *Communications Materials* **1**, 78 (2020).
- [39] Zhao, J. *et al.* Exciton polariton interactions in van der waals superlattices at room temperature. *Nature Communications* **14**, 1512 (2023).

- [40] Raja, A. *et al.* Coulomb engineering of the bandgap and excitons in two-dimensional materials. *Nature communications* **8**, 15251 (2017).
- [41] Jülich Supercomputing Centre. Juwels cluster and booster: Exascale pathfinder with modular supercomputing architecture at juelich supercomputing centre. *Journal of large-scale research facilities* **7** (2021). URL <http://dx.doi.org/10.17815/jlsrf-7-183>.

Supplementary Information:
Optical Readout of Reconfigurable Layered Magnetic Domain Structure in CrSBr

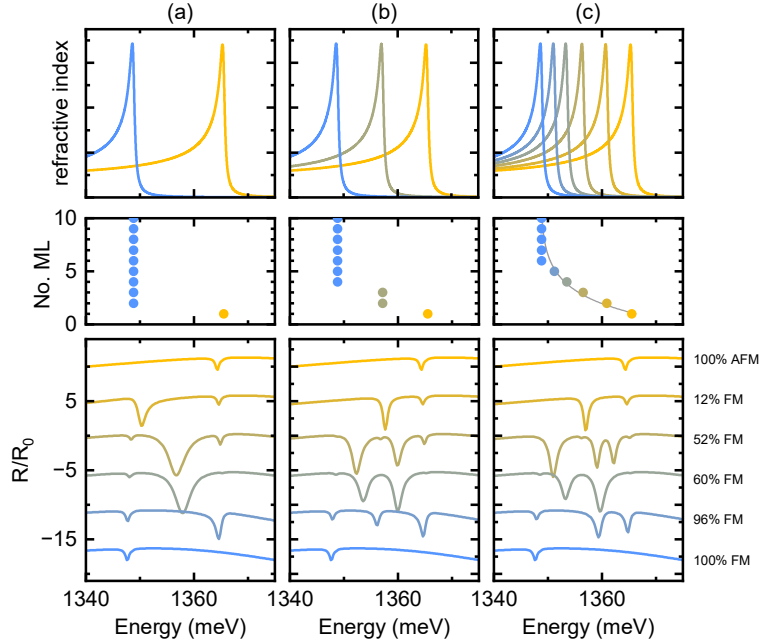


Fig. S1 Comparison between three different approaches to the construction of the dielectric function used in the calculations, along with the subsequent result of the model. In each column: the top row shows the dispersion of the refractive index $n(E)$; the middle row shows the energy of the excitonic resonance depending on the number of layers, all other than energy parameters of the excitonic resonance used to the construction of the dielectric function are the same. The bottom row shows the normalized reflectance R/R_0 for exemplary configurations of AFM/FM stacks with different FM content (given in %). First approach (a) is differing only the monolayer exciton energy (AFM state) and FM state (the number of layers ≥ 2). Even with this simple model we can observe characteristics of the intermediate AFM/FM stack — occurrence of more features in the spectrum and blueshifts. (b) The second approach with additional intermediate energy for thin layers (2–3L); The approach presented in (c) was used in the main paper.

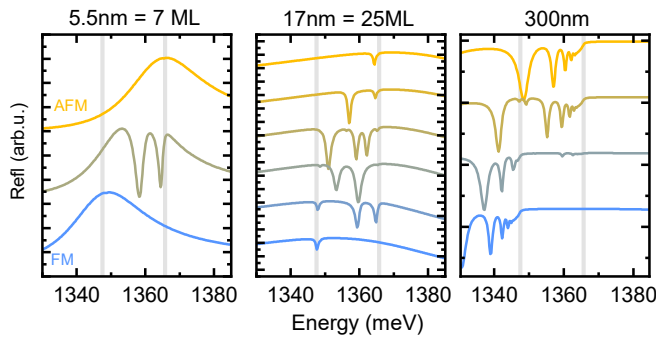


Fig. S2 Left: calculated reflectance spectra for flakes of 7 ML, 25 ML, and 300 nm thickness. Spectra are shown for the pure AFM (top), FM (bottom) and intermediate states between. For 7 ML, the sequence corresponds to one AFM layer sandwiched between two ferromagnetic layers with thickness of 4 (top) and 2 (bottom). For 25 ML and 300 nm, representative mixed configurations are presented. The content of the FM layers is increasing from top (AFM) to bottom (FM) of the graphs.

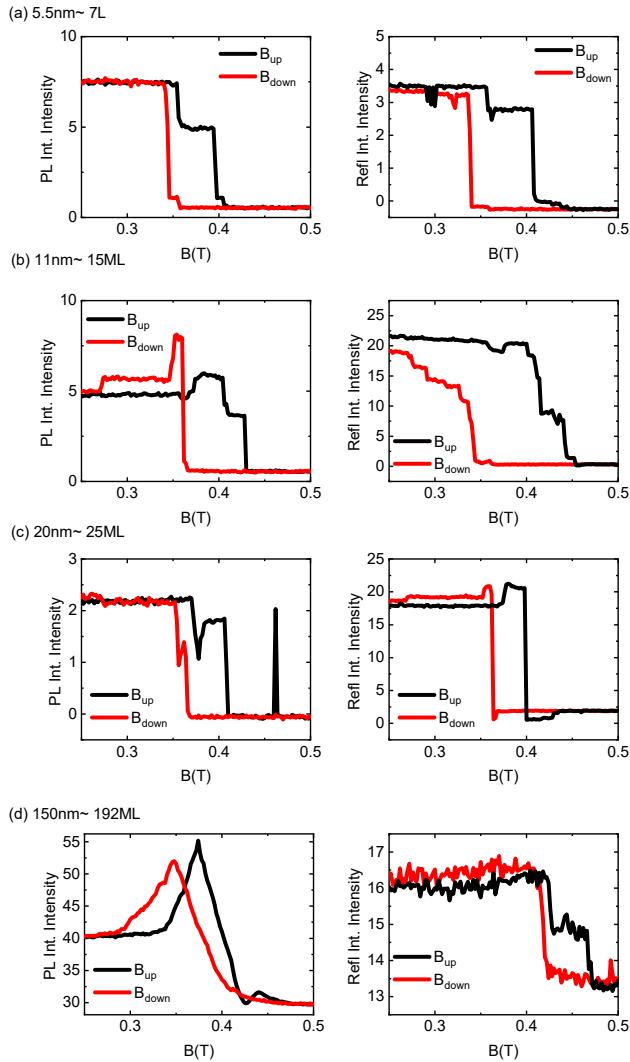


Fig. S3 Integrated signal for the AFM exciton range vs. applied magnetic field of different direction (increasing – black and decreasing – red) for different thicknesses of the flakes for photoluminescence and reflectance scans. Such integrated intensity can give information about number of switches in the intermediate magnetic state region and the range of the magnetic field of such.

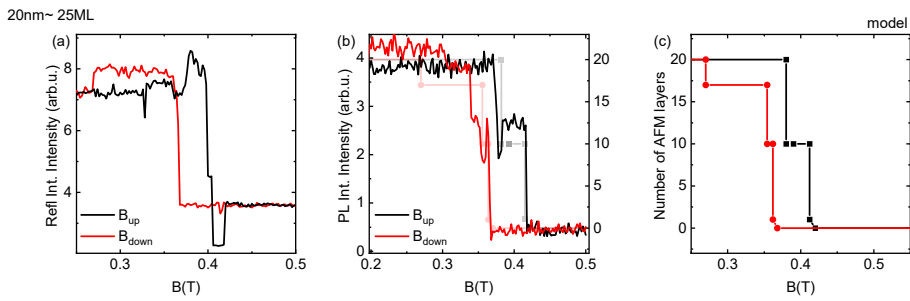


Fig. S4 Integrated signal for the AFM exciton range vs. applied magnetic field of different direction (increasing – black and decreasing – red) for a 20 nm flake: reflectance (a) and photoluminescence (b). Underneath measured data in faint lines is presented the graph (c) which represents the number of AFM layers obtained from the model. That suggests that in the calibrated system the intermediate state can be read out without direct fitting.

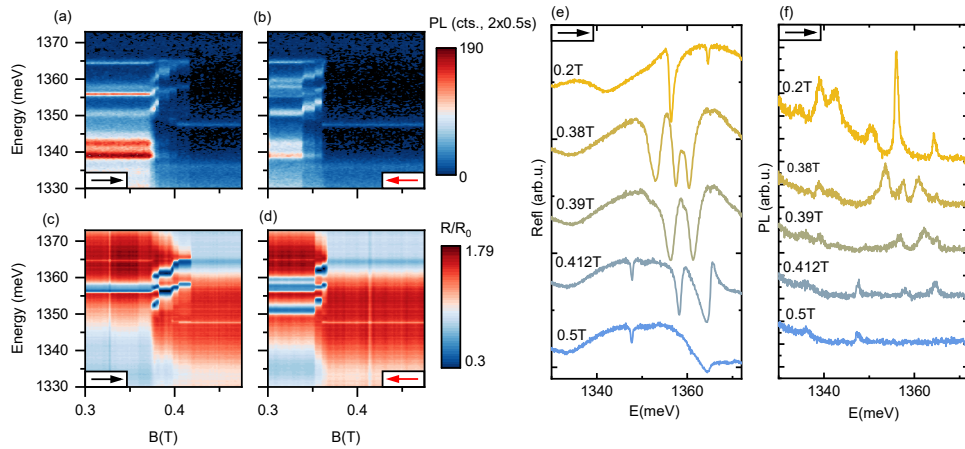


Fig. S5 Comparison between photoluminescence (a,b) and reflectance (c,d) scans for a 20 nm sample for increasing (left) and decreasing (right) external magnetic field. On the right-hand side panels exemplary spectra taken from the increasing scans are presented both for reflectance (e) and photoluminescence (f). Scans in the same direction of the magnetic field give complementary PL and reflectance spectra.